JOURNAL OF GEOPHYSICAL RESEARCH, VOL. 114, D09216, doi:10.1029/2008JD010596, 2009

Forecasting and nowcasting improvement in cloudy regions with high temporal GOES sounder infrared radiance measurements

Zhenglong Li,[1] Jun Li,[1] W. Paul Menzel,[1] James P. Nelson III,[1] Timothy J. Schmit,[2] Elisabeth Weisz,[1] and Steven A. Ackerman[1]

Received 12 June 2008; revised 22 January 2009; accepted 4 March 2009; published 13 May 2009.

[1] In an effort to extend the high temporal resolution Geostationary Operational Environmental Satellite (GOES) infrared sounding retrievals from clear to cloudy skies, a synthetic regression-based cloudy sounding retrieval algorithm has been developed and applied to GOES 12 sounder measurements. Comparisons against radiosondes at the Atmospheric Radiation Measurement Program at Southern Great Plains site from August 2006 to May 2007 and the conventional radiosondes network over the continental United States from January 2007 to November 2008 both show that the retrievals of moisture under thin cloud conditions perform similarly to those under the clear-sky conditions. The largest improvements are found in the upper level integrated precipitable water vapor (PW) or PW3. Also in the case of low thick clouds, PW3 is usually improved significantly. In addition, the retrieved cloud parameters are consistent with the false RGB composite images. With the addition of the soundings under low thick or thin cloud conditions, the area without soundings is reduced by 57% in the selected case. The application to a tornadic storm on 24 April 2007 reveals that the GOES cloudy sounding retrievals are more useful at the early stage of the storm, when nearby clouds are considered thin or broken. The GOES cloudy sounding algorithm reveals more pronounced and extensive convective instability, and it does so earlier than the clear-sky-only results. The cloudy sounding retrievals have the potential to provide an earlier warning to forecasters.

Citation: Li, Z., J. Li, W. P. Menzel, J. P. Nelson III, T. J. Schmit, E. Weisz, and S. A. Ackerman (2009), Forecasting and nowcasting improvement in cloudy regions with high temporal GOES sounder infrared radiance measurements, *J. Geophys. Res.*, *114*, D09216, doi:10.1029/2008JD010596.

1. Introduction

[2] Remote sensing of the weather conditions from satellite sounders has been useful to weather forecasters in two different ways. The derived products from the Geostationary Operational Environmental Satellite (GOES) sounders with high temporal resolution are able to depict early stages of weather system development [*Menzel et al.*, 1998; *Schmit et al.*, 2002; *Li et al.*, 2008]. More quantitatively, data assimilation of the sounder derived products or the measured radiances has proven to improve numerical weather prediction (NWP) [*McNally et al.*, 2006].

[3] There are mainly two kinds of sounder instruments, infrared (IR) and microwave. Typically, IR sounders have better spatial resolution than microwave sounders, and thus are more capable of depicting the mesoscale structures. But, IR radiances are affected by cloud scattering and absorption in cloudy skies; therefore, the usage of IR sounder measurements usually focuses on clear skies.

[4] Extending the use of IR measurements into cloudy regions would be a welcome enhancement. As pointed out by *Wylie et al.* [1994], completely clear-sky observations from the High-Resolution Infrared Radiation Sounder (HIRS, 17.4 km at nadir) occur only 23% during the 4 years of observations, globally. New hyperspectral instruments, such as the Atmospheric Infrared Sounder (AIRS, 13.5 km at nadir), reveal even less clear-sky observations; the chance for a footprint to be clear is less than 10% (H.-L. Huang, and W. L. Smith, Apperception of clouds in AIRS data, paper presented at ECMWF Workshop on Assimilation of High Spectral Resolution Sounders in NWP, European Centre for Medium-Ranger Weather Forecasts, 2004). Studies also show that cloudy regions are more important for NWP error development [*McNally*, 2002] and exhibit more forecast error than clear skies.

[5] Different methods have been developed to extract useful information in cloudy regions. Cloud clearing [*Joiner and Rokke*, 2000; *Li et al.*, 2005b; *Cho and Staelin*, 2006] has been used to derive clear radiances within a partly cloudy field of view (FOV). A basic assumption of cloud clearing is that the differences of earth surface/atmosphere conditions between adjacent FOVs are small. Using sounders with other collocated measurements, for example, combining AIRS with the Moderate Resolution Imaging

[1]Cooperative Institute for Meteorological Satellite Studies, University of Wisconsin–Madison, Madison, Wisconsin, USA.
[2]Center for Satellite Applications and Research, National Environmental Satellite, Data, and Information Service, NOAA, Madison, Wisconsin, USA.

0148-0227/09/2008JD010596$09.00

Spectroradiometer (MODIS) measurements [*Li et al.*, 2005b], or AIRS with the Advanced Microwave Sounding Unit (AMSU) measurements [*Susskind et al.*, 2003; *Cho and Staelin*, 2006], it is possible to derive the equivalent clear radiances within a partly cloudy AIRS FOV. When it is overcast, combining the IR and microwave measurements [*Chevallier et al.*, 2002], enables simultaneous retrieval of atmospheric profiles and cloud parameters. This method is especially useful when clouds are opaque as demonstrated by H.-L. Huang and W. L. Smith (An extension of the simultaneous TOVS retrieval algorithm—The inclusion of cloud parameters, paper presented at Third International TOVS Study Conference, International Association of Meteorology and Atmospheric Physics, Madison, Wisconsin, 1986). These methods focus on removing the effect of clouds so that atmospheric soundings can be achieved. Another method is to identify channels unaffected by clouds within a specific FOV [*McNally and Watts*, 2003]. For a hyperspectral IR instrument, even when clouds are present, some channels are not affected by the clouds. Channels peaking in upper troposphere do not "see" lower clouds, and thus are able to provide useful atmospheric information above the clouds.

[6] Recent studies [*Weisz et al.*, 2007; *Zhou et al.*, 2007] show hyperspectral IR measurements are able to retrieve atmospheric profiles along with cloud parameters in two conditions. One, when clouds are optically thin, the observed IR radiation includes a contribution from below the cloud down to the surface. With the simultaneously retrieved cloud information, such as cloud top pressure (CTP), cloud optical thickness (COT) and cloud effective particle size, the algorithm is able to account for the cloud effect and retrieve the temperature and moisture profile information. Second, when clouds are optically thick, contribution below clouds is hidden, but soundings above the clouds can be retrieved.

[7] This study focuses on thin clouds (defined as having retrieved COT smaller than 2.0) and low thick clouds (defined as having retrieved CTP larger than 850 hPa and retrieved COT larger than 2.0). In this paper, optically thin clouds include high thin cirrus clouds and some low-level clouds that could be regarded as thin in this study. When a FOV is only partly covered by scattered low clouds, the effective optical thickness is not large. Even low stratus clouds or other thick clouds, at cloud edge, are considered as thin clouds for increasing sounding coverage. According to *Warren et al.* [1985], low clouds have an occurrence frequency of 15% between 30° and 60°N. *Chang and Li*'s [2005] study shows the global single-layer cirrus clouds have an occurrence frequency of 12% under cloudy conditions.

[8] The current GOES sounders (GOES 8/9/10/11/12/13) have been measuring radiances in 18 IR spectral bands since 1994, from approximately 3.7 to 14.7 μm, over the continental United States (CONUS) and adjacent oceanic regions. The hourly radiance measurements along with the derived products have been helpful in short-term nowcasting and forecasting in clear skies [*Menzel et al.*, 1998; *Ma et al.*, 1999; *Li et al.*, 2008]. The 10 km footprint size suggests that extension of sounding retrievals from clear to cloudy skies would greatly increase sounding coverage. This paper presents a new cloudy retrieval algorithm and applications with GOES 12 sounder measurements. Table 1 shows the instrument's characteristics and primary purpose of each channel of GOES sounder. Among the 18 IR channels, only the first 15 channels are used for cloudy soundings.

[9] Section 2 provides details about the cloudy retrieval algorithm. Validations of the cloudy retrievals against radiosonde observations (RAOB) are presented in section 3. Analysis of retrieved cloud parameters is presented in section 4. Application of the retrievals in a severe storm case is shown in section 5. A summary is given in section 6.

2. GOES Cloudy Sounding Retrieval Algorithm

[10] Unlike the physical retrieval algorithm for clear skies [*Li et al.*, 2008], the GOES single FOV (SFOV) cloudy sounding algorithm starts with a statistical linear regression technique. This method was first introduced by *Smith et al.* [1970]. A summary for cloudy sounding retrievals follows.

[11] Sounding retrieval pursues a relationship between satellite measurements and atmospheric soundings, or

$$Y(n) = K(n,m)X(m) \tag{1}$$

where $Y(n)$ is a vector of retrieval parameters (n unknowns, including cloud, surface and atmosphere parameters), $X(m)$ is a vector of measurements (m knowns, including satellite measurements and other known variables), and $K(n, m)$ is an operator matrix to calculate Y given X. With a training database, the regression coefficients can be obtained using the least square method

$$K = YX^T\left(XX^T\right)^{-1} \tag{2}$$

[12] In this study, the synthetic regression [*Seemann et al.*, 2003] is used. The GOES 12 sounder IR measurements are simulated radiances calculated from a radiative transfer model. The predictors for the linear regression algorithm include (1) the brightness temperature (Tb) and the quadratic terms (Tb^2) of the first 15 IR channels, (2) surface pressure, (3) local zenith angle, (4) observed surface air temperature and moisture if available (following the work by *Ma et al.* [1999], *Li et al.* [2000], W. L. Smith et al. (The simultaneous retrieval export package, paper presented at the Second International TOVS Study Conference, Cooperative Institute for Meteorological Satellite Studies, Igls, Austria, 1985), and W. L. Smith and H. M. Woolf (A linear simultaneous solution for temperature and absorbing constituent profiles from radiance spectra, paper presented at the Fourth International TOVS Study Conference, Cooperative Institute for Meteorological Satellite Studies, Igls, Austria, 1988)), and (5) the forecast profiles of temperature and moisture [*Li et al.*, 2008]. The predictants include (1) profiles of temperature, moisture and ozone, (2) surface skin temperature, (3) COT at 0.55 μm, and (4) CTP. Separate sets of regression coefficients are generated for water and ice clouds. More details about the predictors and predictants are given in the following subsections.

2.1. Training Database and Cloud Top Determination

[13] In the training process, the GOES IR radiances are calculated with given profiles of temperature, moisture and

Table 1. GOES 8–13 Sounder Instrument Characteristics and Primary Purpose

Wave Range	Channel	Wavelength (μm)	Band	Purpose
Long-wave IR	1	14.71	carbon dioxide	stratosphere T
Long-wave IR	2	14.37	carbon dioxide	tropopause T
Long-wave IR	3	14.06	carbon dioxide	upper level T
Long-wave IR	4	13.64	carbon dioxide	midlevel T
Long-wave IR	5	13.37	carbon dioxide	low level T
Long-wave IR	6	12.66	water vapor	surface T, W
Long-wave IR	7	12.02	window	surface T, W
Medium-wave IR	8	11.03	window	surface T
Medium-wave IR	9	9.71	ozone	total ozone
Medium-wave IR	10	7.43	water vapor	low level W
Medium-wave IR	11	7.02	water vapor	midlevel W
Medium-wave IR	12	6.51	water vapor	upper level W
Short-wave IR	13	4.57	carbon dioxide	low level T
Short-wave IR	14	4.52	carbon dioxide	midlevel T
Short-wave IR	15	4.45	carbon dioxide	upper level T
Short-wave IR	16	4.13	nitrogen	boundary layer T
Short-wave IR	17	3.98	window	surface T
Short-wave IR	18	3.74	window	surface T, W

ozone, sensor's view angle, surface skin temperature, surface pressure, surface emissivities, CTP, 0.55 μm COT, and effective particle size, using the equation for radiative transfer [*Zhou et al.*, 2007]

$$R = R_0 F_T \tau_{tc} + R_c \tau_{tc} + R_1 + R_1^{\downarrow} F_R \tau_{tc} \quad (3)$$

where R is upwelling radiance at the top of the atmosphere. R_0, R_c, R_1, and $R_1^{\downarrow}$ are upwelling emission below the cloud, emission from the cloud, upwelling emission from the atmosphere above the cloud, and downwelling emission from the atmosphere above the cloud, respectively. F_T and F_R are the cloud transmissive and reflective functions. τ_{tc} is the transmittance between the cloud and the top of the atmosphere. The upwelling emission R_0 includes the surface emission, the atmospheric upwelling emission below the cloud, and the downwelling emissions by the cloud and the atmosphere (both above and below the cloud), which are reflected back to the space by the surface.

[14] The SeeBor training database (E. Borbas et al., Global profile training database for satellite regression retrievals with estimates of skin temperature and emissivity, paper presented at 14th International ATOVS Study Conference, NASA, Beijing, 2005) contains about 15000 global profiles of temperature, moisture and ozone from National Oceanic and Atmospheric Administration (NOAA)-88, the European Centre for Medium-Range Weather Forecasts (ECMWF), the Thermodynamic Initial Guess Retrieval-3 (TIGR-3), ozonesondes, and desert radiosondes. A physically based characterization of surface skin temperatures and surface IR emissivities are included in this database. Most profiles are from clear-sky conditions. In order to generate the cloudy profiles, clouds are added at a selected level. Figure 1a shows the thresholds of relative humidity (RH) used to select the level where clouds are added. Working from the top to the surface, clouds are added at a level when the RH is larger than the given threshold. The purpose of these thresholds is to distribute the clouds evenly at all heights. In our approach, ice clouds are added between

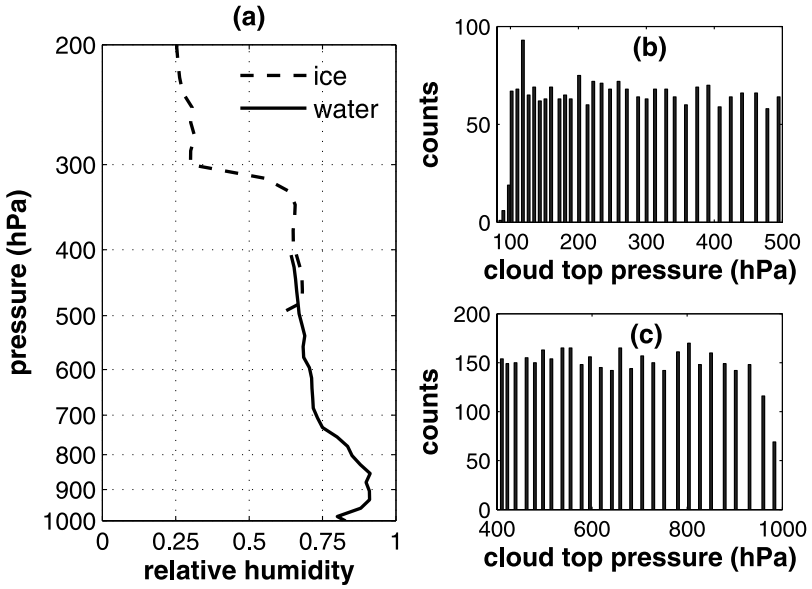

Figure 1. (a) Two profiles of RH thresholds to determine where to add clouds, (b) the histogram of ice cloud top pressure in the training, and (c) the histogram of water cloud top pressure in the training.

100 and 500 hPa; water clouds are added between 400 hPa and the surface. Figures 1b and 1c show the histograms of the CTP assigned to the cloudy profiles in training data sets for ice and water clouds, respectively.

[15] Among the 15000 profiles, 2162 suitable profiles are found where ice clouds can be added and 4017 for water clouds. The clouds are added with a random value of cloud optical thickness (COT) from [0.01, 0.1, 0.2, 0.5, 1.0, 1.5, 2.0, 3.0, 4.5, 6.5, and 10.0]. The training set is classified into 10 different satellite view angles (note this is not local zenith angle) classes appropriate for the GOES 12 sounder (3.5, 4.0, 4.5, 5.0, 5.5, 6.0, 6.5, 7.0, 7.5, and 8.0). For each view angle, random values between x − 0.25° and x + 0.25° are assigned. For ice clouds, the effective particle size in diameter (De) is obtained using [*Heymsfield et al.*, 2003]

$$De = \frac{A \cdot \tau^{\alpha}}{\tau - B \cdot \tau^{\alpha}}, A = 18.7652, B = 0.32522, \alpha = 1.1905 \quad (4)$$

where τ is COT at 0.55 μm. As suggested by *Li et al.* [2005a], a 10% random variation is added to De, and the final value is restricted to be between 10 and 50 μm. For water clouds, sensitivity studies by *Li et al.* [2005a] show that De could be randomly assigned between 5 and 35 μm, with a mean of 30 μm, and a standard deviation (STD) of 10 μm.

2.2. Radiative Transfer Model

[16] The Pressure-Layer Fast Algorithm for Atmospheric Transmittance (PFAAST) model [*Hannon et al.*, 1996] is applied to calculate the clear-sky GOES 12 sounder radiances. PFAAST is based on the Line By Line Radiative Transfer Model (LBLRTM) version 8.4 [*Clough and Iacono*, 1995] and the high-resolution transmission molecular absorption database-2000 (HITRAN-2000) [*Rothman et al.*, 1992] with updates (aer_hitran_2000_updat_01.1).

[17] The cloudy radiances are calculated by coupling the clear-sky optical thickness from PFAAST with the associated COT at 0.55 μm. The COT is calculated with a fast radiative transfer cloud model developed by University of Wisconsin–Madison (UW) and Texas A&M University [*Baum et al.*, 2000; *Wei et al.*, 2004]. The original model, designed for hyperspectral IR sounders, is adapted to the GOES 12 sounder. In this model, the bulk single-scattering properties of ice crystals are calculated by assuming aggregates for large particles (>300 μm), hexagonal geometries for moderate particles (50–300 μm) and droxtals for small particles (0–50 μm); the water cloud droplet is assumed to be spherical and the classical Lorenz-Mie theory is used to calculate the single-scattering properties.

[18] The surface IR emissivities are assumed to be 0.98 in cloudy skies.

2.3. Constructing Forecast Error Profile

[19] The forecast temperature and moisture profiles are used as predictors for the retrievals by providing extra profile information [*Li et al.*, 2008]. Since there are no forecast data in the SeeBor database, the forecast error profiles have to be constructed to simulate the forecast data.

[20] A separate match-up database is used to derive the forecast error profile; it contains RAOBs, the GOES 12 sounder Tbs and the National Center for Environmental Prediction (NCEP) Global Forecast System (GFS) model forecast profiles from June 2003 to September 2004 over the CONUS. One difficulty in constructing a forecast error profile is that temperature/moisture at one level is highly correlated with those from nearby levels. In order to characterize the correlation in the error profiles, a principle component analysis (PCA) is applied.

[21] From the match-up database, a set of forecast error profiles U are obtained. Then the PCA is performed on U

$$U = E \times \Lambda \quad (5)$$

where $E = [E_1 \quad E_2 \quad \cdots \quad E_m]$ represents the eigenvectors, and m is the number of eigenvectors. Λ is the matrix set of eigenvalues. For each error profile U_i (i = 1, n, where n is the number of profiles), we have

$$U_i = E \times \Lambda_i \quad (6)$$

where $\Lambda_i = \begin{bmatrix} \Lambda_{i1} \\ \Lambda_{i2} \\ \vdots \\ \Lambda_{im} \end{bmatrix}$ are the eigenvalues for the ith error profile. The jth eigenvalue Λ_{ij} corresponds to the jth eigenvector E_j. Both the eigenvectors and the eigenvalues are arranged in the order of relative importance with the most important eigenvalue/vector as the first one. Statistical analysis is performed on all the eigenvalues to get the mean and the STD, which are used to generate random numbers as eigenvalues, which in turn are used to simulate the forecast error profiles. Because the nearby levels are correlated, it is not necessary to have all the eigenvalues and vectors to reconstruct each profile. Using 90% of the data set as training and other 10% for validation, Figure 2 shows 15 temperature and 9 moisture eigenvectors are sufficient to construct 95% of the variance of the forecast error profiles. Except around 200 hPa, where the temperature is highly variable near the tropopause, the constructed error profiles have similar bias and root mean square (RMS) as the original ones.

2.4. Cloud Phase Determination

[22] Two sets of Tb are calculated, one with ice and the other with water cloud regression coefficients. The Tb closer to the observed Tb (smaller residuals) is chosen and cloud phase is assigned accordingly.

2.5. Noise Reduction and Bias Adjustment

[23] Noise reduction is done differently under cloudy than clear-sky conditions. In the case of clear sky, the inverted cone method [*Li et al.*, 2008; *Plokhenko and Menzel*, 2001] is used, where more opaque spectral band radiances are averaged over larger areas to reduce noise. Under cloudy conditions, because of (1) the large radiance contrast between clear and cloudy regions and (2) the nonhomogeneousness of cloud tops, a 3 by 3 FOV averaging method is used to reduce the radiance noise:

$$\overline{R}(m,n) = \frac{\sum_{j=-1}^{1}\sum_{i=-1}^{1} R(m+i,n+j)\cdot K(m+i,n+j)}{\sum_{j=-1}^{1}\sum_{i=-1}^{1} K(m+i,n+j)} \quad (7)$$

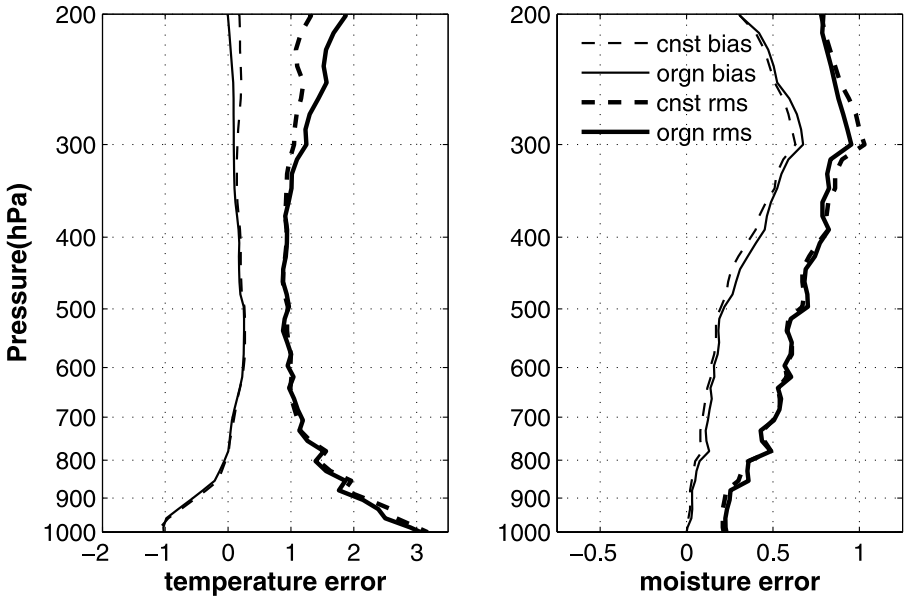

Figure 2. The original (orgn) and constructed (cnst) bias and RMS of forecast error profiles. (left) The temperature is in K, and (right) the moisture is in logarithm of mixing ratio (g/Kg). The thin dashed line is the constructed bias profile, the thin solid line is the original bias profile, the thick dashed line is the constructed RMS profile, and the thick solid line is the original RMS profile.

where $\overline{R}(m, n)$ is the averaged radiance at location (m, n), $R(m+i, n+j)$ is the measured radiance at location $(m+i, n+j)$, and $K(m+i, n+j)$ equals 1 if the FOV is cloudy or 0 if it is clear.

[24] A radiance bias adjustment is also necessary. Radiance biases are the result of changes in radiometer performance and calibration, and uncertainty of radiative transfer model. Changes over time in bias are caused by radiometer performance drift. Figure 3 shows how the GOES 12 sounder's biases have changed with time. For June 2003 to September 2004, most channels have biases less than 2.0 K except channel 15, which has a bias of about 5 K. For August 2006 to May 2007, biases calculated from clear cases in the RAOB/GOES/GFS-ARM database (see section 3) are somewhat larger. In this study, the biases are simply removed by deducting the averaged biases. Note for channel 1, 2, 10, 11, 12, 14 and 15, the STD of the 2006–2007 bias is smaller than the 2003–2004 bias. This is because the inverted cone method is used to filter the noise in the newer match-up database for the clear cases; the simple 3 by 3 radiance averaging is used in the older one. Although the noise reduction does not reduce the average of the biases, it reduces the STD of the biases.

3. Validation

[25] Two different data sets of temperature and moisture profiles are used for validation. The first one is the RAOB data from August 2006 to May 2007, collected from the U.S. Department of Energy Atmospheric Radiation Measurement (ARM) Program at Southern Great Plains (SGP) site at Lamont, OK (C1, 36°37′N, 97°30′W). The second is the conventional RAOB over the CONUS from January 2007 to November 2008. They are both spatially and temporally collocated with the GOES 12 sounder measurements and NCEP GFS forecast profiles to form two match-up databases. The first is referred as the RAOB/GOES/GFS-ARM match-up database, and the second as the RAOB/GOES/GFS match-up database. The collocation conditions are (1) spatial distance smaller than 10 km and (2) temporal distance smaller than half an hour. In the first, 765 collocated samples have been obtained, in which 362 are cloudy. In the second, 53037 collocated samples have been obtained, in which 21607 are cloudy.

[26] The ARM RAOB data are listed separately from the conventional RAOB because they are more frequent (4 times a day), and have better overall quality than the conventional

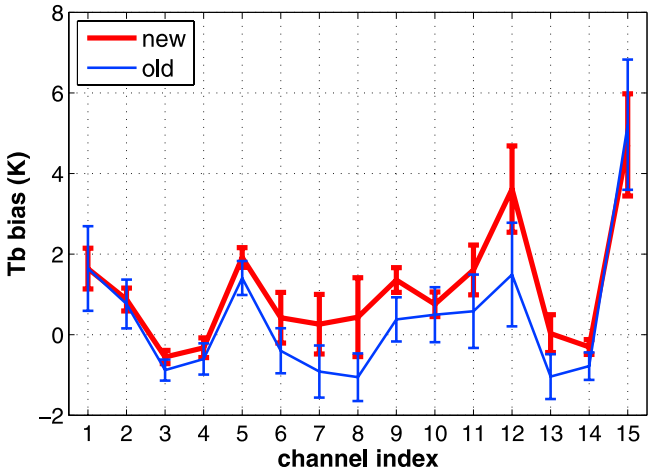

Figure 3. The averaged biases for GOES 12 sounder's first 15 IR channels. The old bias (thin blue line) is from June 2003 to September 2004. The new bias (thick red line) is from August 2006 to May 2007. The bar at each point represents the standard deviation of the bias.

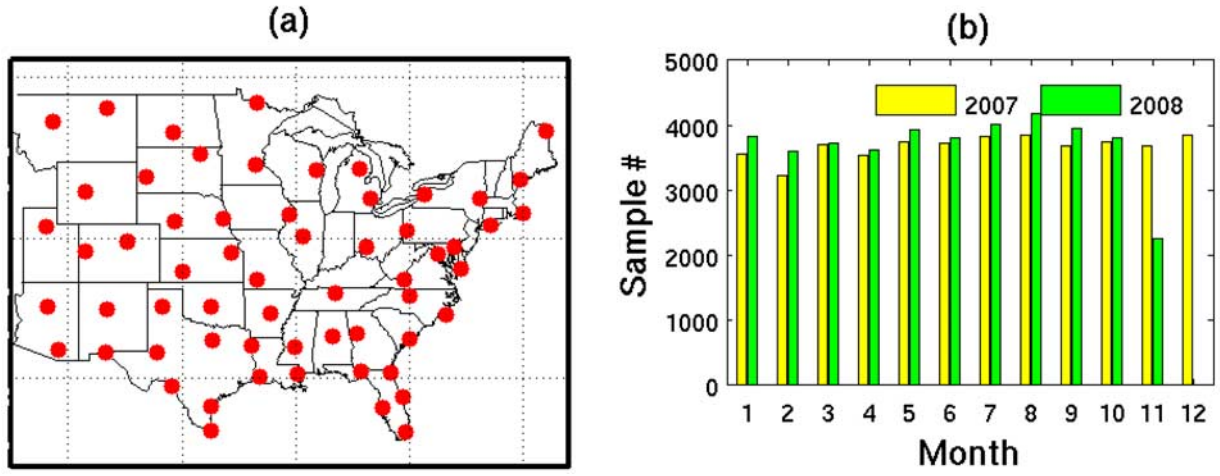

Figure 4. (a) The radiosonde station locations over the CONUS in the RAOB/GOES/GFS match-up database and (b) monthly sample distribution.

RAOB [*Turner et al.*, 2003]. The sampling rate is 2 s through the flight. For each sample output, details about time in seconds and quality flag are provided. Experiences at the Cooperative Institute for Meteorological Satellite Studies (CIMSS)/UW have shown that the GOES sounding retrievals agree with ARM RAOB better than with the conventional RAOB [*Miloshevich et al.*, 2006]. Therefore, the RAOB/GOES/GFS-ARM match-up database will be used as the primary database for validation. However, validation against conventional RAOB is also presented because it is the only way to demonstrate that the algorithm works under different weather and surface conditions. Figure 4 shows the station location and monthly sample distribution of the collected conventional RAOB.

3.1. Determination of Thin Clouds

[27] Sounding retrievals below optically thick clouds are not attempted because there is little information from beneath the clouds. A threshold COT of 2.0 has been set and clouds with COT larger than 2.0 are not considered for profile retrieval in the whole atmospheric column; for low thick clouds, retrievals above cloud top are performed.

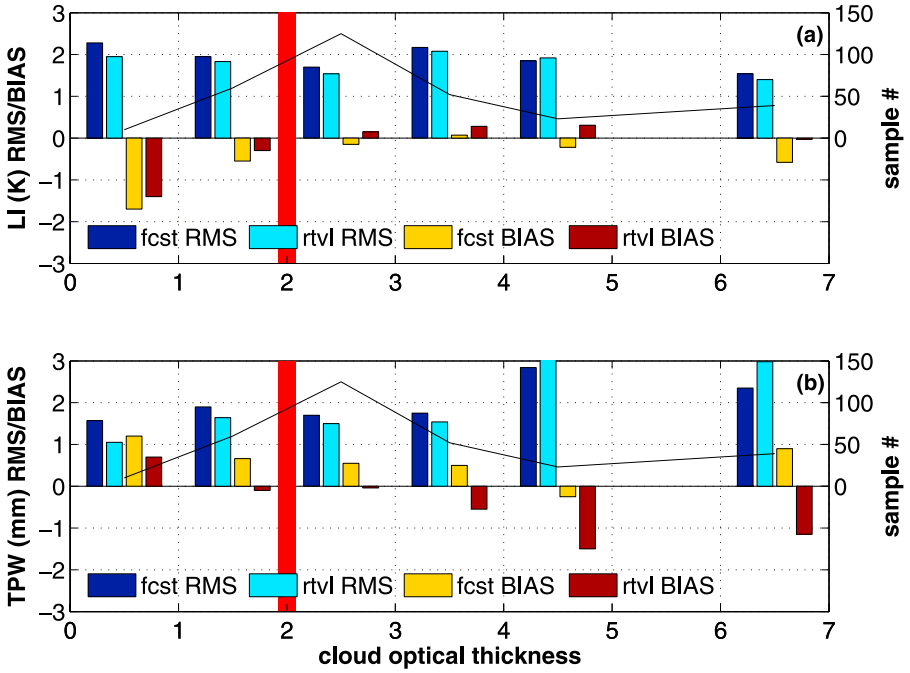

Figure 5. Validation of (a) lifted index and (b) total precipitable water against RAOB for different cloud optical thickness using the RAOB/GOES/GFS-ARM match-up database. The dark and light blue bars represent the RMS of the forecast and the cloudy retrievals, respectively. The yellow and dark red bars represent the bias of the forecast and the cloudy retrievals, respectively. The black solid line shows the sample distribution as a function of cloud optical thickness.

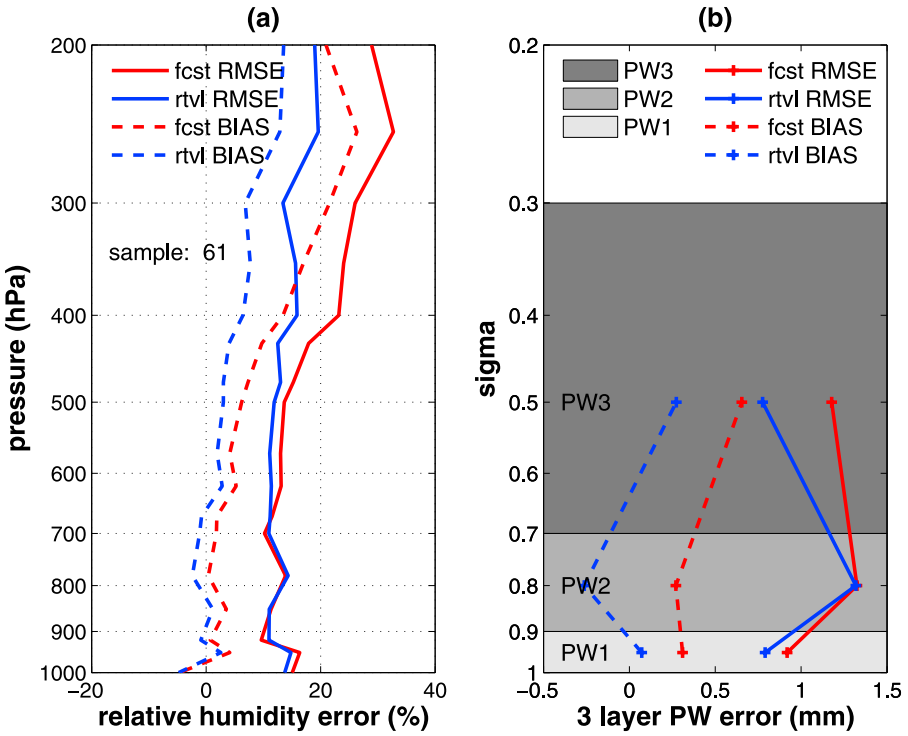

Figure 6. Error profiles of (a) relative humidity and (b) three-layer PW for thin clouds with retrieved COT less than 2.0 using RAOB/GOES/GFS-ARM match-up database. The dashed red line represents NCEP GFS forecast bias, the solid red line represents NCEP GFS forecast RMS, the dashed blue line represents cloudy retrieval bias, and the solid blue line represents cloudy retrieval RMS. The shaded areas in Figure 6b show the vertical coverage for each PW.

[28] Figure 5 shows how the RMS and bias of retrieved total precipitable water (TPW) and the lifted index (LI) change with the COT using the RAOB/GOES/GFS-ARM match-up database. As the clouds get thinner, the retrieval improvement over forecast, as shown by the RMS and bias, gets more significant. In this study, the COT of 2.0 was selected for the threshold to determine soundings under thin cloud conditions, which has 61 samples in Figure 5 (or 17% of cloudy FOVs). One might argue that 2.5 even 3.0 is still a good threshold from Figure 5, and a larger threshold will ensure more cloudy retrievals. But the main reason 2.0 is chosen is because low water clouds with the same COT are more difficult to retrieve than high ice clouds. Whether the retrieval algorithm is sensitive to cloud parameters depends on the derivative of the radiance to the COT. A large value indicates large sensitivity and promises better retrievals. Low clouds typically exhibit little temperature contrast between the surface and the cloud top. Therefore, with the same COT, low clouds introduce more retrieval errors than ice clouds.

3.2. Validation of Cloudy Sounding Retrievals Using ARM RAOB

[29] Our validation focuses on moisture, especially the RH profile and three-layer PW. The three-layer PW is integrated precipitable water in sigma coordinates. PW1 is from the surface to 0.9 (roughly 900 hPa), PW2 is from 0.9 to 0.7 (roughly 900 to 700 hPa), and PW3 is from 0.7 to 0.3 (roughly 700 to 300 hPa). In other words, the three-layer PW depicts the moisture in the lower, middle and upper troposphere.

3.2.1. Thin Clouds

[30] A typical NCEP GFS forecast RH error profile [*Divakarla et al.*, 2006] has smaller error in the lower troposphere (RMS is around 20%) than the middle troposphere (RMS is around 35%) and the upper troposphere (RMS is around 50%) as compared with RAOB. There is little bias for pressure greater than 400 hPa, and less than 15% for pressure less than 400 hPa.

[31] Figure 6a shows the RH error profile under thin cloud conditions. At the ARM SGP site, the GFS forecast has an RMS of 15% in the lower troposphere (pressure greater than 500 hPa), and 35% in the upper troposphere. After the retrieval, all RMS magnitudes decrease. Around 250 hPa, the improvement by the cloudy retrieval algorithm is the largest; the RMS is reduced to about 20%. Going closer to the surface, the improvement is smaller. From 700 to 1000 hPa, it is hard to see any improvement. Figure 6b shows the three-layer PW in sigma coordinate. As expected, PW3 is improved significantly; both the RMS and the bias are reduced. PW1 has some improvements although not as much as PW3. PW2 is not improved in RMS or bias.

[32] There are only four significant moisture sensitive channels (channel 6, 10, 11 and 12) on the GOES 12 sounder (see Table 1). Figure 7a shows the moisture weighting functions (which show the relative contributions to the radiance measurements by different layer of moisture) of the four channels calculated for the U.S. Standard Atmosphere 1976; channel 6 (12.66 μm) peaks around 800 hPa, channel 10 (7.43 μm) around 600 hPa, channel 11 (7.02 μm) around 400 hPa, and channel 12 (6.51 μm)

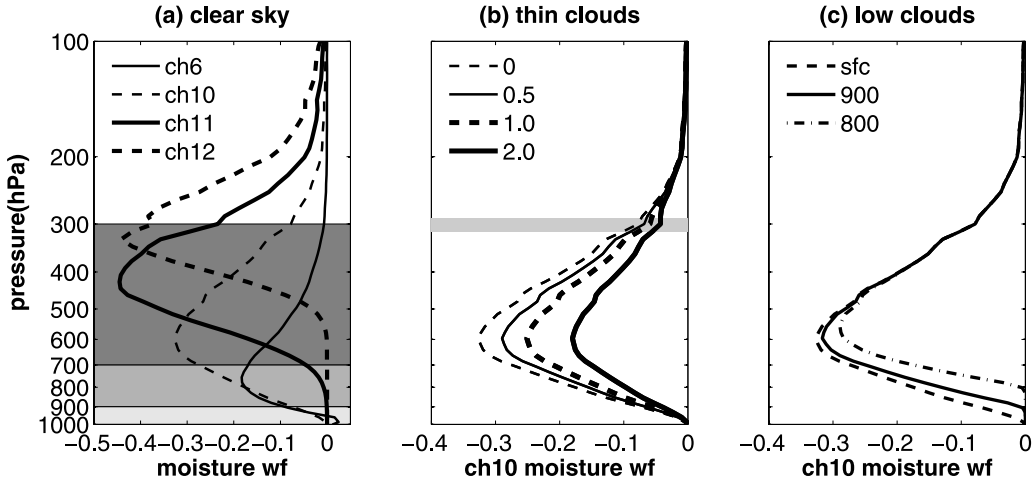

Figure 7. GOES 12 sounder's moisture weighting functions for (a) channels 6, 10, 11, and 12 under clear skies; (b) channel 10 under thin clouds with different cloud optical thickness; and (c) channel 10 under opaque clouds with different cloud top pressure. The shaded areas in Figure 7a corresponds to the coverage of three-layer PWs (see Figure 6). The shaded line in Figure 7b is where the cloud top relies. The U.S. standard Atmosphere 1976 is used.

around 300 hPa. Thus, channel 10, 11 and 12 are likely to influence PW3 which allows the largest improvement. Only channel 6 and 10 have some influence on PW2. PW2 has some improvement depending on the location of the weighting functions; if the atmosphere becomes wet, the moisture weighting functions move upward, and PW2 is unlikely to be improved. Semitransparent clouds also affect the amplitude of the weighting functions, hence the influence in thin clouds of channel 10 on PW2 retrieval (as shown in Figure 7b). In thin clouds there is less improvement in PW2. Channel 6, together with channel 7 (not shown), contain PW1 boundary layer moisture information. But more importantly, the hourly surface observations, used as the predictors, account for most of the improvement in the PW1 retrieval.

3.2.2. Low Thick Clouds

[33] Under low thick cloud conditions (defined as retrieved CTP greater than 850 hPa and retrieved COT greater than 2.0), the NCEP GFS forecast performs very well (see Figure 8a); the RH RMS is less than 10% between 500 and 600 hPa, and less than 20% from 850 to 200 hPa. Figure 8a shows that the retrieval algorithm is able to improve the forecast moisture profile above the cloud top. Again, larger improvement is found in the upper troposphere than in the lower troposphere. In Figure 8b, PW3 and PW2 have significant improvement; but PW1, even with surface observations, does not show any improvement at all.

[34] In this study, the difference between the low thick clouds and the thin clouds is that the former could be regarded as thick in the spectrum of IR. Radiation from below the clouds is negligible. It is like the surface is being lifted to the height of the effective cloud top (referred to as the lifted surface assumption in this paper). This has the largest impact on channel 6 and 10. Figure 7c shows the moisture weighting function of channel 10 by using the lifted surface assumption (channel 6 should see the same effect). Although the magnitude decreases a little above the cloud top, the disappearance below the clouds sharpens the weighting function, which actually increases the sensitivity above the clouds. Thus the retrieval of PW2 and PW3 can be expected to show improvement.

[35] To explore the lifted surface assumption, the clear-sky physical retrieval algorithm [*Li et al.*, 2008] is performed for low thick cloud conditions by placing the surface at the height of CTP, which has been retrieved from the cloudy retrieval algorithm. The GFS forecast is used as first guess. The green lines in Figure 8a show the clear-sky retrievals with surface at CTP are a little better (roughly 5% RH improvement below 400 hPa) than the cloudy ones. This suggests another viable approach to extract profile information above the low thick clouds would be to use clear retrievals with the surface lifted to the CTP.

3.3. Validation of Cloudy Sounding Retrievals Using Conventional RAOB Network

[36] Previous validations were from RAOBs at one location. In this section, the validations include many locations using the RAOB/GOES/GFS match-up database. Figure 9 shows the bias and RMS differences of the moisture profiles as compared with RAOB. The results here are very similar to those in Figures 6a and 8a. Under the thin cloud conditions, the largest improvements are in the upper troposphere; both the RH and the mixing ratio show significant improvements. In the middle troposphere, the improvements are small with respect to RH, but substantial with respect to mixing ratio. In the lower troposphere, the improvements become more substantial, especially with respect to the mixing ratio. In the case of low thick clouds, the largest improvements are in the upper troposphere too. And the improvements become less significant in the lower troposphere, as the impacts by the clouds become more significant.

[37] Statistical comparisons of other moisture or moisture related products are shown in Table 2. For each product, four statistical parameters are shown: the correlation coefficient (R), the RMS, the bias and the standard devia-

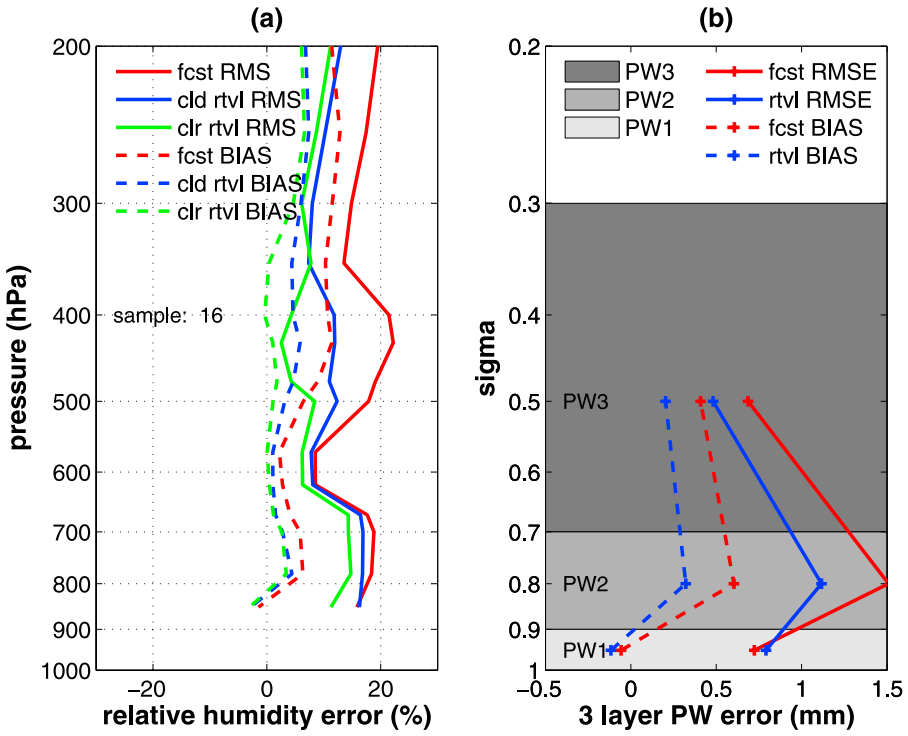

Figure 8. Same as Figure 6 except for low thick clouds with retrieved CTP larger than 850 hPa and retrieved COT larger than 2.0. The green lines show the clear-sky physical retrieval results with surface placed at the effective cloud top.

tion (STD). The samples are categorized into 3 groups of conditions: "clear" represents all the successfully retrieved clear-sky samples, "low" represents all the successfully retrieved cloudy samples with retrieved CTP larger than 850 hPa and retrieved COT larger than 2.0; "thin" represents all the successfully retrieved cloudy samples with the retrieved COT less than 2.0. LI, TPW and PW1 retrievals in low thick clouds are not attempted.

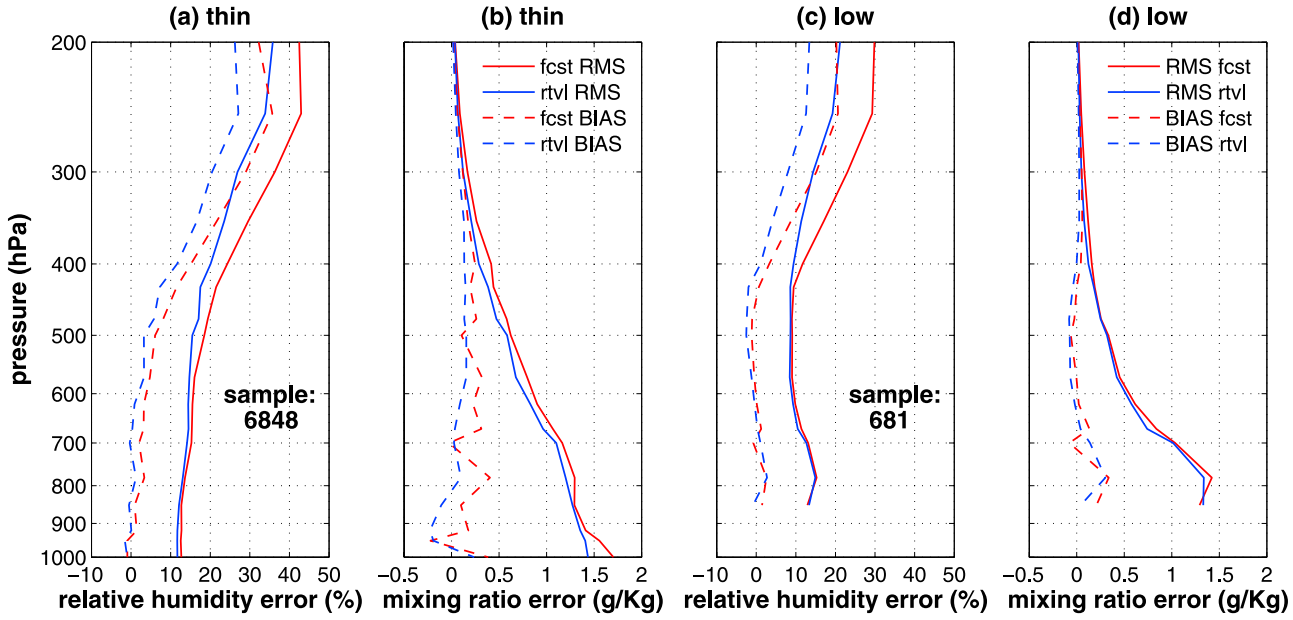

Figure 9. Validation of moisture profiles using RAOB/GOES/GFS match-up database: (a) relative humidity under thin clouds conditions, (b) mixing ratio under thin clouds conditions, (c) relative humidity under low thick clouds conditions, and (d) mixing ratio under low thick clouds conditions. The blue lines represent retrievals, and the red lines represent the NCEP GFS forecast. The dashed lines represent the biases, and the solid lines represent the RMS.

Table 2. Correlation Coefficient, RMS, Bias, and Standard Deviation of LI, TPW, PW1, PW2, and PW3 Under Different Conditions as Compared With the Conventional RAOB Using the RAOB/GOES/GFS Match-Up Database From January 2007 to November 2008[a]

	LI		TPW		PW1		PW2		PW3	
	GFS	RTVL	GFS	RTVL	GFS	RTVL	GFS	RTVL	GFS	RTVL
R										
Clear	0.974	0.977	0.972	0.974	0.969	0.973	0.959	0.959	0.919	0.926
Low	N/A	N/A	N/A	N/A	N/A	N/A	0.884	0.882	0.460	0.471
Thin	0.977	0.979	0.973	0.975	0.969	0.974	0.959	0.959	0.925	0.933
RMS										
Clear	2.08	1.95	3.19	3.05	1.26	1.17	1.79	1.76	1.43	1.28
Low	N/A	N/A	N/A	N/A	N/A	N/A	2.08	2.00	1.31	1.24
Thin	2.10	2.06	3.51	3.24	1.25	1.22	1.93	1.89	1.79	1.47
Bias										
Clear	0.568	0.565	0.418	0.220	−0.241	−0.116	0.293	0.229	0.550	0.391
Low	N/A	N/A	N/A	N/A	N/A	N/A	0.425	0.297	0.078	−0.066
Thin	0.574	0.662	0.839	−0.090	−0.201	−0.335	0.414	−0.006	0.840	0.462
SD										
Clear	2.01	1.87	3.16	3.05	1.24	1.16	1.76	1.75	1.32	1.22
Low	N/A	N/A	N/A	N/A	N/A	N/A	2.03	1.98	1.31	1.24
Thin	2.02	1.95	3.41	3.24	1.24	1.17	1.89	1.89	1.58	1.40

[a]"Clear" represents all the successful retrievals under clear skies, "low" represents all the successful cloudy retrievals with the retrieved CTP larger than 850 hPa and COT larger than 2.0, and "thin" represents all the successful cloudy retrievals with the retrieved COT less than 2.0. R, correlation coefficient; SD, standard deviation.

[38] Columns 4 and 5 in Table 2 shows the results of TPW. Under both clear-sky and thin cloud conditions, the retrievals show better TPW products than the GFS forecast. The correlation coefficients increase. The STD, RMS and bias decrease. Columns 6–11 in Table 2 shows the statistical results of PW1, PW2 and PW3. Again, the results are similar to those in Figures 6b and 8b. The improvements of moisture decrease from the upper troposphere to the lower troposphere. Near the surface, the surface observations improve the retrieval. It is interesting that PW2 gets improved in terms of RMS under all the three conditions. However, this improvement is not substantial considering the correlation coefficients do not increase and the STD does not decrease much. The reason that the STD of low thick clouds has the largest decrease of 0.05 mm is because the atmosphere tends to be dry in low thick cloud conditions over land (TPW smaller than 30 mm, not shown). As noted before, less moisture results in more PW2 improvement.

[39] Columns 2 and 3 in Table 2 show the results of LI. In both clear-sky and thin cloud conditions, the algorithm is able to produce better LI than the GFS forecast; the correlation coefficients increase; the STD and the RMS decrease. But the algorithm fails to decrease the bias under the thin cloud conditions; the reason for this is still under investigation.

[40] Previous analysis shows the overall performance by the retrieval algorithm. To study the performance for different TPWs, Figure 10 shows how the RMS and the bias of the moisture products change with the TPW under the thin cloud conditions. Only the thin cloud cases are shown here because the low thick cloud cases are limited (less than 4% of the cloud cases). From Figures 10d and 10f, the retrieval of PW1 and PW3 is not significantly affected by the total moisture content; the retrieval algorithm improves the first guess no matter what TPW is. For PW2 (Figure 10e), if the atmosphere is dry or TPW is smaller than 30 mm, the retrieval algorithm improves the first guess. But, if the atmosphere is wet or TPW is larger than 40 mm, the retrieval algorithm fails to improve the first guess. This is consistent with the discussion in section 3.2.1.

[41] Figure 10b shows how the RMS and the bias of the LI change with the TPW. It is interesting that the algorithm fails to improve LI when TPW is less than 20 mm. However, this is probably not significant for severe storm nowcasting, because most of the severe storms happen in the vicinity of areas with large TPW. Figure 11 shows the scatterplot of the density between the TPW and the LI, both of which are calculated from RAOB. When TPW is smaller than 20 mm, LI is almost always greater than 0. Although the improvement of LI is not significant, the increased coverage is of more importance.

4. Analysis of Retrieved Cloud Parameters

[42] The cloudy algorithm retrieves not only the profile information in cloudy regions, but also the cloud parameters. In this section, an example of retrieved cloud parameters will be shown and interpreted with the help from the false RGB image. It should be noted that this section is not an attempt to validate CTP or phase product, as done by *Hollars et al.* [2004] and *Hawkinson et al.* [2005]. The validation will be one of the future work.

[43] Figure 12 shows the derived product imagery (DPI) of the retrieved cloud parameters at 1800 UTC on 13 April 2006, or 4 h before the outbreak of a severe thunderstorm with large hail and damaging downburst winds. Figure 12a is the false RGB image using R = 0.65 μm, G = 3.9–11 μm and B = 11 μm flipped (note this is a daytime case). The clear sky is green with the water darker (sea) or bluer (great lakes) than the land. The light red or light yellow regions are low clouds. The pink or white areas are high clouds.

[44] Figure 12b shows the retrieved CTP. The high clouds appear blue and low clouds appear red in the image. The CTP values agree qualitatively with the RGB image. The

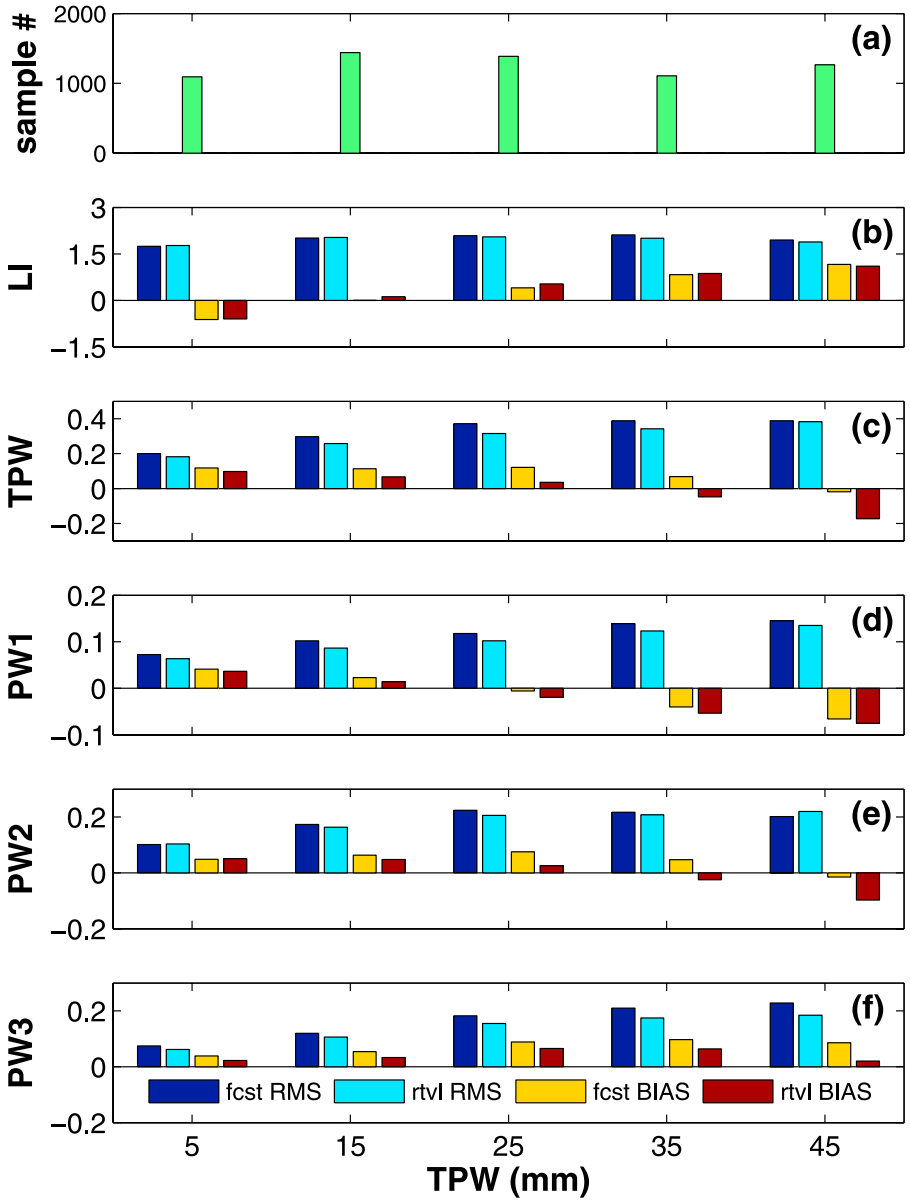

Figure 10. Validation of moisture products under the thin cloud conditions at different TPW level using RAOB/GOES/GFS match-up database. (a) The sample distribution, (b) LI, (c) TPW, (d) PW1, (e) PW2, and (f) PW3. The dark and light blue bars represent the RMS of the forecast and the cloudy retrievals, respectively. The yellow and dark red bars represent the bias of the forecast and the cloudy retrievals, respectively.

thin cirrus clouds over the New Mexico, west Minnesota and central Michigan are retrieved with CTP less than 400 hPa. Some high clouds on top of the low clouds over the sea (Gulf of Mexico and to the east of Florida) are also identified correctly. Most of the low clouds have CTP larger than 700 hPa. There are two large low cumulus cloud regions over south Texas and southwest Arkansas; most have CTP greater than 700 hPa, but some appear to be well developed with CTP less than 500 hPa.

[45] Most of the cloud phase (Figure 12c) also agrees with the RGB image. But the algorithm underestimates the coverage by ice clouds. For example, both the RGB and the CTP show there is a cirrus cloud band extending from Florida to the east of Bahamas, but the cloud phase image shows it being ice clouds mixed with water clouds. The cloud phase determination is difficult in two situations. If the clouds are mixed phase or the ice (water) clouds are too low (high), the water and ice cloud retrieval might have comparable residuals, making it hard to determine the phase. If there are multiple-layer clouds and the cirrus clouds on top are too thin, the algorithm will not be able to identify the thin cirrus clouds either.

[46] Figure 12d shows the additional coverage accomplished with cloudy soundings, reducing the nonretrieval area by 57%. The low thick cloud retrievals (light blue) are those with the retrieved CTP larger than 850 hPa and the retrieved COT larger than 2.0. Most of them are over the sea. The thin cloud retrievals are those with the retrieved

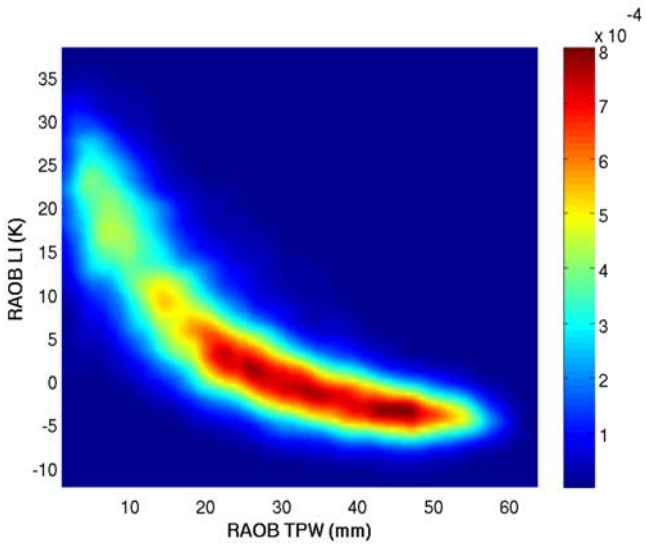

Figure 11. The scatterplot of density between TPW and LI calculated from RAOBs in RAOB/GOES/GFS match-up database. Notice LI is almost always greater than 0 when TPW is smaller than 20 mm.

COT less than 2.0. The green color represents the low thin (lthin) clouds with CTP larger than 500 hPa, and the yellow color represents the high thin (hthin) clouds with CTP less than 500 hPa. Figure 12e shows the histogram of these thin clouds. About half of them are hthin (mostly thin cirrus clouds) with CTP less than 500 hPa. Others are mostly low clouds with CTP greater than 700 hPa. These clouds are mostly low broken clouds. As a result, they appear more scattered than the hthin in Figure 12d. The "other" category in Figure 12d includes clouds with COT larger than 2.0 and CTP less than 850 hPa, moisture retrievals in these cloud conditions were not validated in this study.

5. Applications to a Severe Storm Case

[47] The GOES 12 sounder IR imagery around Eagle Pass, Texas on 24 April 2007 reveal three individual storms within 6 h. The first storm, a supercell, initialized around 2015 UTC; the second storm happened between 2200 and 2300 UTC to the north of the supercell; and the third storm (not shown) happened between 0100 and 0200 UTC of the next day to the west of the supercell. A tornado was observed within the supercell around 0000 UTC on 25 April 2007 at Eagle Pass, Texas. This EF-3 tornado killed

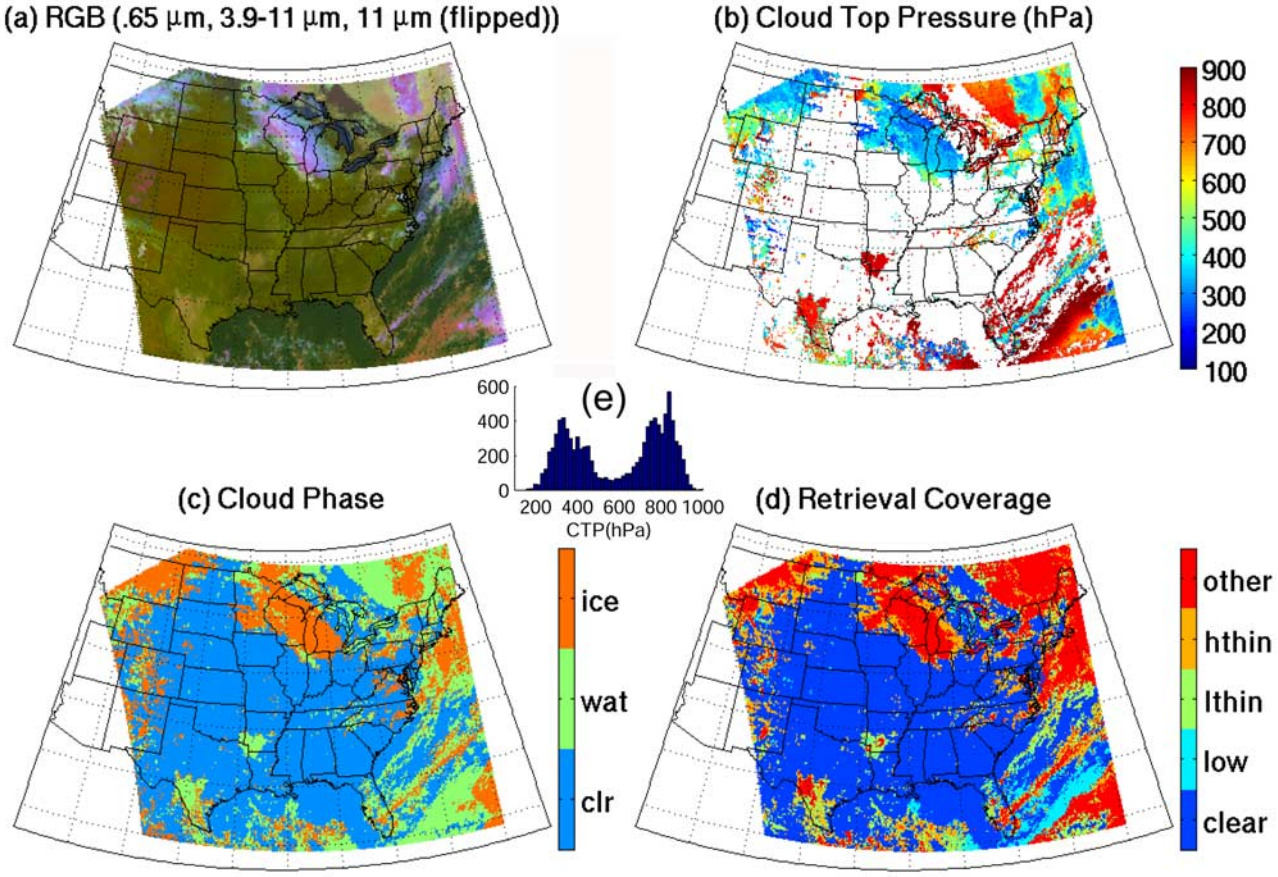

Figure 12. The derived product imagery of the retrieved cloud parameters at 1800 UTC on 13 April 2006. (a) The false color RGB image (R = 0.65 μm, G = 3.9–11 μm and B = 11 μm flipped); (b) the cloud top pressure; (c) the cloud phase; (d) the retrieval coverage; and (e) the histogram of CTP of thin clouds with COT smaller than 2.0. Thin clouds with CTP larger than 500 hPa are represented by lthin, and thin clouds with CTP smaller than 500 hPa are represented by hthin.

10 people in Mexico and the United States with another 120 injured. *Li et al.* [2008] demonstrated clear-sky GOES soundings improving the first guess of the GFS forecast for this storm.

[48] Figure 13 shows the results of the time sequence of the LI retrieved from clear and some cloudy FOVs. Shown are 2000 UTC (Figures 13a–13d), 2100 UTC (Figures 13e–13h), 2200 UTC (Figures 13i–13l), and 2300 UTC (Figures 13m–13p). Figures 13a, 13e, 13i, and 13m show the NCEP GFS forecast; Figures 13b, 13f, 13j, and 13n show the Rapid Update Cycle (RUC [*Benjamin et al.*, 2004]) 6-h forecast; Figures 13c, 13g, 13k, and 13o show GOES 12 clear-sky retrievals; and Figures 13d, 13h, 13l, and 13p show GOES 12 clear plus cloudy retrievals. The retrievals are indicated by LI values, with different colors representing different values. Otherwise, 11 μm Tb values are shown, most of which are in cloudy regions with COT greater than 2.

[49] The regional model, RUC, performs better than the coarse global model, GFS, on this severe storm case. During the 4 h, the GFS forecast model failed to predict the convective instability surrounding the supercell, while the RUC successfully did so. The locations of the convective instability are to the southeast or southwest of the convective storms, as expected from the prevailing wind flow.

[50] The clear-sky retrievals (Figures 13c, 13g, 13k, and 13o) successfully identify three large areas of instability. As shown in Figure 13o, area A is located to the northwest of the supercell, area B is located to the southwest of the supercell, and area C is located to the south of the supercell. Each of these areas is associated with convective activity. The clear plus cloudy retrievals (Figures 13d, 13h, 13l, and 13p) have better coverage than the clear-sky retrievals; more convective instability is found in areas B and C. More importantly, before the clear-sky retrievals indicate any large instability areas, the cloudy retrievals have identified some areas in the cloudy regions. The earliest convective instability revealed by the clear plus cloudy retrievals was around 1900 UTC or about 75 min before the super cell outbreak.

[51] The RUC 6-h forecast appears to have a similar performance as the clear plus cloudy retrievals (comparing Figures 13b, 13f, 13j, and 13n with Figures 13d, 13h, 13l, and 13p); both reveal the convective instability in area A. And these instabilities are associated with the second convective storm. Careful examination reveals that the RUC differs from the clear plus cloudy retrievals to the south of the supercell. Both the clear and the cloudy retrievals identify areas B and C consistently and continuously. The RUC picks up area B at 2000 and 2100 UTC, but it fails completely at 2200 UTC in Figure 13j. And the instabilities at 2300 UTC in Figure 13n are too far away from the supercell. The RUC completely misses area C, which is associated with the third convective storm. It is not until the outbreak of the third convective storm that the RUC picks up area C (not shown). The GOES sounder provides additional useful information beyond the RUC for the forecasters in this severe storm case. According to *Benjamin et al.* [2004], high-frequency moisture observations above the surface used in the RUC analysis are TPW (and CTP) from satellites (such as GOES sounder, Special Sensor Microwave Imager and GPS). The disadvantage of these observations is lack of vertical information. As a result, it is hard for RUC to predict when and where a storm is likely to form.

6. Summary

[52] The large probability that a GOES sounder measurement is affected by clouds prompted this study to extend the clear-sky retrievals to cloudy regions. A synthetic regression-based cloudy retrieval algorithm is developed and applied to GOES 12 sounder radiance measurements. To complement the limited profile information from GOES 12 sounder's first 15 IR channels, the GFS forecast profiles, and hourly surface observations are included as predictors.

[53] Cloudy retrievals are attempted in (1) thin clouds, defined as having cloud optical thickness COT < = 2.0, and (2) low thick clouds, defined as having cloud top pressure CTP > = 850 and COT > = 2.0.

[54] Comparisons with the RAOBs at the ARM SGP site from August 2006 to May 2007 and the conventional RAOBs from January 2007 to November 2008, show that under thin cloud conditions moisture retrievals are of similar quality to clear-sky retrievals. The largest improvements are found in the upper atmosphere. Going down to the middle troposphere, the improvements diminish. However, in the boundary layer, the moisture retrieval is usually improved with the help from the surface observations.

[55] The low thick clouds have a different impact. The opaqueness of low thick clouds blocks the radiation from below the clouds and neutralizes the help of hourly surface observations. As a result, the boundary layer moisture is hardly improved. However, the weighting functions above the cloud top are sharpened. Together with the fact that the atmosphere is usually dry under the low thick cloud conditions, the middle troposphere moisture retrieval is improved.

[56] The retrieved cloud parameters compare well with the false RGB (0.65 μm, 3.9–11 μm and 11 μm flipped) image; the high clouds have small CTP and are classified as ice clouds and the low clouds have large CTP and are classified as water clouds. The additional sounding retrievals in low thick clouds and thin clouds reduce the nonretrieval area by 57% in the selected case.

[57] The cloudy retrieval algorithm was applied to a tornadic severe storm case on 24 April 2007; the cloudy retrievals were especially useful during the early stages of the storms, when the nearby clouds were usually broken/low/thin clouds. There are three areas of convective instability in this case, which are associated with subsequent activity. The clear-sky retrievals are able to identify the three areas, but the additional cloudy retrievals improve the early identification with more pronounced and extensive instability in the three areas. These earlier and stronger warnings should be important for forecasters.

[58] While the Rapid Update Cycle (RUC) forecast model reveals more convective instability than the GFS model on this severe storm case, the retrievals, both in clear and cloudy skies, locate the convective instability more accurately to the south (or southeast/southwest) of the individual storms. These results are especially encouraging considering the fact that some of the operational GOES sounder products (clear-sky TPW and CTP) are already assimilated into the RUC.

[59] Overall, the results presented in this study are felt to be promising. For forecasters, the new cloudy retrievals

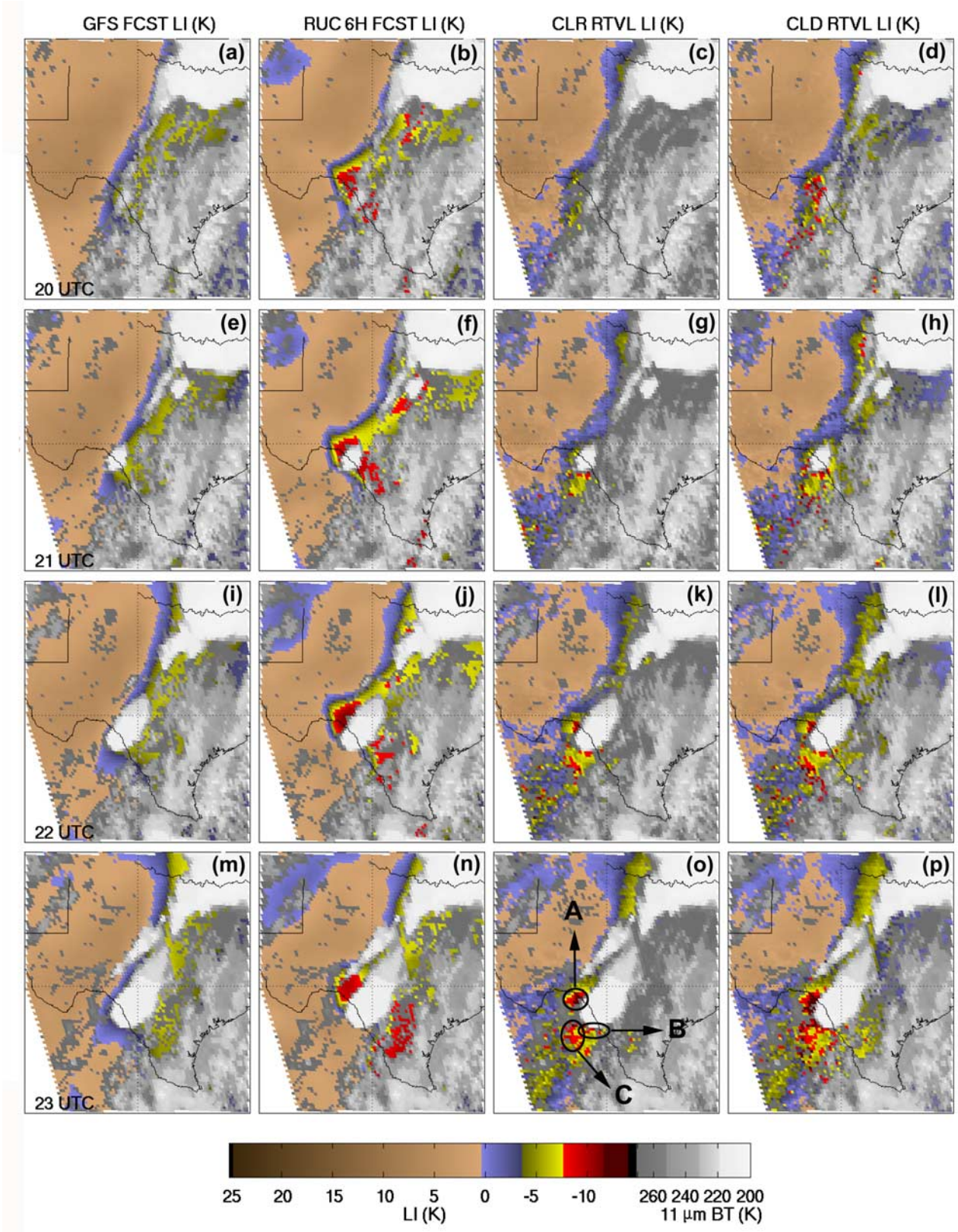

Figure 13. Time series of the derived product imagery of LI on 24 April 2007 at (a–d) 2000 UTC, (e–h) 2100 UTC, (i–l) 2200 UTC, and (m–p) 2300 UTC. Figures 13a, 13e, 13i, and 13m are for the GFS forecast; Figures 13b, 13f, 13j, and 13n are for the RUC 6-h forecast; Figures 13c, 13g, 13k, and 13o are for GOES 12 clear-sky retrievals; and Figures 13d, 13h, 13l, and 13p are for GOES 12 clear plus cloudy retrievals. Note that the two areas A and B are each associated with convective activity. The area C is associated with a third storm which happened between 0100 and 0200 UTC on 25 April 2007.

can provide nowcasting products with better coverage for monitoring weather development. For modelers, the retrieved cloud parameters, as well as the profile information, are complementary to the NWP models.

[60] **Acknowledgments.** The authors would like to thank Hal Woolf for providing the 101-level PFAAST radiative transfer model for GOES 12 sounder. Some data were obtained from the Atmospheric Radiation Measurement (ARM) Program sponsored by the U.S. Department of Energy, Office of Science, Office of Biological and Environmental Research, Environmental Sciences Division. This program is supported at CIMSS by NOAA GIMPAP program NA06NES4400002 and GOES-R program NA07EC0676. The views, opinions, and findings contained in this report are those of the authors and should not be construed as an official National Oceanic and Atmospheric Administration or U.S. Government position, policy, or decision.

References

Baum, B. A., P. F. Soulen, K. I. Strabala, M. D. King, S. A. Ackerman, W. P. Menzel, and P. Yang (2000), Remote sensing of cloud properties using MODIS Airborne Simulator imagery during SUCCESS. II. Cloud thermodynamic phase, *J. Geophys. Res.*, *105*, 11,781–11,792, doi:10.1029/1999JD901090.

Benjamin, S. G., et al. (2004), An hourly assimilation-forecast cycle: The RUC, *Mon. Weather Rev.*, *132*(2), 495–518, doi:10.1175/1520-0493(2004)132<0495:AHACTR>2.0.CO;2.

Chang, F., and Z. Li (2005), A near-global climatology of single-layer and overlapped clouds and their optical properties retrieved from Terra/MODIS data using a new algorithm, *J. Clim.*, *18*(22), 4752–4771, doi:10.1175/JCLI3553.1.

Chevallier, F., P. Bauer, J.-F. Mahfouf, and J.-J. Morcrette (2002), Variational retrieval of cloud profile from ATOVS observations, *Q. J. R. Meteorol. Soc.*, *128*(585), 2511–2525, doi:10.1256/qj.01.153.

Cho, C., and D. H. Staelin (2006), Cloud clearing of Atmospheric Infrared Sounder hyperspectral infrared radiances using stochastic methods, *J. Geophys. Res.*, *111*, D09S18, doi:10.1029/2005JD006013.

Clough, S. A., and M. J. Iacono (1995), Line-by-line calculations of atmospheric fluxes and cooling rates: 2. Applications to carbon dioxide, ozone, methane, nitrous oxide and the halocarbons, *J. Geophys. Res.*, *100*, 16,519–16,535, doi:10.1029/95JD01386.

Divakarla, M. G., C. D. Barnet, M. D. Goldberg, L. M. McMillin, E. Maddy, W. Wolf, L. Zhou, and X. Liu (2006), Validation of Atmospheric Infrared Sounder temperature and water vapor retrievals with matched radiosonde measurements and forecasts, *J. Geophys. Res.*, *111*, D09S15, doi:10.1029/2005JD006116.

Hannon, S., L. L. Strow, and W. W. McMillan (1996), Atmospheric infrared fast transmittance models: A comparison of two approaches, *Proc. SPIE Int. Soc. Opt. Eng.*, *2830*, 94–105.

Hawkinson, J. A., W. Feltz, and S. A. Ackerman (2005), A comparison of GOES sounder- and cloud lidar- and radar-retrieved cloud-top heights, *J. Appl. Meteorol.*, *44*(8), 1234–1242, doi:10.1175/JAM2269.1.

Heymsfield, A. J., S. Matrosov, and B. Baum (2003), Ice water path–optical depth relationships for cirrus and deep stratiform ice cloud layers, *J. Appl. Meteorol.*, *42*, 1369–1390, doi:10.1175/1520-0450(2003)042<1369:IWPDRF>2.0.CO;2.

Hollars, S., Q. Fu, J. Comstock, and T. Ackerman (2004), Comparison of cloud-top height retrievals from ground-based 35 GHz MMCR and GMS-5 satellite observations at ARM TWP Manus site, *Atmos. Res.*, *72*(1–4), 169–186, doi:10.1016/j.atmosres.2004.03.015.

Joiner, J., and L. Rokke (2000), Variational cloud-clearing with TOVS data, *Q. J. R. Meteorol. Soc.*, *126*(563), 725–748, doi:10.1002/qj.49712656316.

Li, J., W. Wolf, W. P. Menzel, W. Zhang, H.-L. Huang, and T. H. Achtor (2000), Global soundings of the atmosphere from ATOVS measurements: The algorithm and validation, *J. Appl. Meteorol.*, *39*, 1248–1268, doi:10.1175/1520-0450(2000)039<1248:GSOTAF>2.0.CO;2.

Li, J., H. Huang, C. Liu, P. Yang, T. J. Schmit, H. Wei, E. Weisz, L. Guan, and W. P. Menzel (2005a), Retrieval of cloud microphysical properties from MODIS and AIRS, *J. Appl. Meteorol.*, *44*(10), 1526–1543, doi:10.1175/JAM2281.1.

Li, J., C. Y. Liu, H.-L. Huang, T. J. Schmit, W. P. Menzel, and J. Gurka (2005b), Optimal cloud-clearing for AIRS radiances using MODIS, *IEEE Trans. Geosci. Remote Sens.*, *43*, 1266–1278, doi:10.1109/TGRS.2005.847795.

Li, Z., J. Li, W. P. Menzel, T. J. Schmit, J. P. Nelson III, J. Daniels, and S. A. Ackerman (2008), GOES sounding improvement and applications to severe storm nowcasting, *Geophys. Res. Lett.*, *35*, L03806, doi:10.1029/2007GL032797.

Ma, X. L., T. J. Schmit, and W. L. Smith (1999), A nonlinear physical retrieval algorithm—Its application to the GOES-8/9 sounder, *J. Appl. Meteorol.*, *38*(5), 501–513, doi:10.1175/1520-0450(1999)038<0501:ANPRAI>2.0.CO;2.

McNally, A. P. (2002), A note on the occurrence of cloud in meteorologically sensitive areas and the implications for advanced infrared sounders, *Q. J. R. Meteorol. Soc.*, *128*(585), 2551–2556, doi:10.1256/qj.01.206.

McNally, A. P., and P. D. Watts (2003), A cloud detection algorithm for high-spectral-resolution infrared sounders, *Q. J. R. Meteorol. Soc.*, *129*(595), 3411–3423, doi:10.1256/qj.02.208.

McNally, A. P., P. D. Watts, J. A. Smith, R. Engelen, G. A. Kelly, J. N. Thepaut, and M. Matricardi (2006), The assimilation of AIRS radiance data at ECMWF, *Q. J. R. Meteorol. Soc.*, *132*(616), 935–957, doi:10.1256/qj.04.171.

Menzel, W. P., F. C. Holt, T. J. Schmit, R. M. Aune, A. J. Schreiner, G. S. Wade, and D. G. Gray (1998), Application of GOES-8/9 soundings to weather forecasting and nowcasting, *Bull. Am. Meteorol. Soc.*, *79*(10), 2059–2077, doi:10.1175/1520-0477(1998)079<2059:AOGSTW>2.0.CO;2.

Miloshevich, L. M., H. Voemel, D. N. Whiteman, B. M. Lesht, F. J. Schmidlin, and F. Russo (2006), Absolute accuracy of water vapor measurements from six operational radiosonde types launched during AWEX-G and implications for AIRS validation, *J. Geophys. Res.*, *111*, D09S10, doi:10.1029/2005JD006083.

Plokhenko, Y., and W. P. Menzel (2001), Mathematical aspects in meteorological processing of infrared spectral measurements from the GOES sounder. Part I: Constructing the measurement estimate using spatial smoothing, *J. Appl. Meteorol.*, *40*(3), 556–567, doi:10.1175/1520-0450(2001)040<0556:MAIMPO>2.0.CO;2.

Rothman, L. S., et al. (1992), The HITRAN molecular database: Editions of 1991 and 1992, *J. Quant. Spectrosc. Radiat. Transfer*, *48*, 469–507, doi:10.1016/0022-4073(92)90115-K.

Schmit, T. J., W. F. Feltz, W. P. Menzel, J. Jung, A. P. Noel, J. N. Heil, J. P. Nelson III, and G. S. Wade (2002), Validation and use of GOES sounder moisture information, *Weather Forecast.*, *17*(1), 139–154, doi:10.1175/1520-0434(2002)017<0139:VAUOGS>2.0.CO;2.

Seemann, S., J. Li, W. P. Menzel, and L. Gumley (2003), Operational retrieval of atmospheric temperature, moisture, and ozone from MODIS infrared radiances, *J. Appl. Meteorol.*, *42*, 1072–1091, doi:10.1175/1520-0450(2003)042<1072:OROATM>2.0.CO;2.

Smith, W. L., H. M. Woolf, and W. J. Jacob (1970), A regression method for obtaining real-time temperature and geopotential height profiles from satellite spectrometer measurements and its application to Nimbus 3 "SIRS" observations, *Mon. Weather Rev.*, *98*, 582–603, doi:10.1175/1520-0493(1970)098<0582:ARMFOR>2.3.CO;2.

Susskind, J., C. D. Barnet, and J. M. Blaisdell (2003), Retrieval of atmospheric and surface parameters from AIRS/AMSU/HSB data in the presence of clouds, *IEEE Trans. Geosci. Remote Sens.*, *41*(2), 390–409, doi:10.1109/TGRS.2002.808236.

Turner, D. D., B. M. Lesht, S. A. Clough, J. C. Liljegren, H. E. Revercomb, and D. C. Tobin (2003), Dry bias and variability in Vaisala RS80-H radiosondes: The ARM experience, *J. Atmos. Oceanic Technol.*, *20*(1), 117–132.

Warren, S. G., C. J. Hahn, and J. London (1985), Simultaneous occurrence of different cloud types, *J. Clim. Appl. Meteorol.*, *24*, 658–667, doi:10.1175/1520-0450(1985)024<0658:SOODCT>2.0.CO;2.

Wei, H., P. Yang, J. Li, B. B. Baum, H.-L. Huang, S. Platnick, Y. Hu, and L. Strow (2004), Retrieval of semitransparent ice cloud optical thickness from Atmospheric Infrared Sounder (AIRS) measurements, *IEEE Trans. Geosci. Remote Sens.*, *42*, 2254–2267, doi:10.1109/TGRS.2004.833780.

Weisz, E., J. Li, J. Li, D. K. Zhou, H. Huang, M. D. Goldberg, and P. Yang (2007), Cloudy sounding and cloud-top height retrieval from AIRS alone single field-of-view radiance measurements, *Geophys. Res. Lett.*, *34*, L12802, doi:10.1029/2007GL030219.

Wylie, D. P., W. P. Menzel, H. M. Woolf, and K. I. Strabala (1994), Four years of global cirrus cloud statistics using HIRS, *J. Clim.*, *7*(12), 1972–1986, doi:10.1175/1520-0442(1994)007<1972:FYOGCC>2.0.CO;2.

Zhou, D. K., W. L. Smith, X. Liu, A. M. Larar, S. A. Mango, and H.-L. Huang (2007), Physically retrieving cloud and thermodynamic parameters from ultraspectral IR measurements, *J. Atmos. Sci.*, *64*, 969–982, doi:10.1175/JAS3877.1.

S. A. Ackerman, J. Li, Z. Li, W. P. Menzel, J. P. Nelson III, and E. Weisz, Cooperative Institute for Meteorological Satellite Studies, University of Wisconsin–Madison, 1225 West Dayton Street, Madison, WI 53706, USA. (zhenglong.li@ssec.wisc.edu)

T. J. Schmit, Center for Satellite Applications and Research, National Environmental Satellite, Data, and Information Service, NOAA, 1225 West Dayton Street, Madison, WI 53706, USA.